The Angular and Spectral Kernel Model for BRDF and Albedo Retrieval

Sihan Liu, Qiang Liu, Qinhuo Liu, Jianguang Wen, and Xiaowen Li

***Abstract*—Albedo may be derived from clear-sky remote-sensing images through inversion of a bidirectional reflectance distribution function (BRDF) model and angular integration. This paper proposes a new multi-angular and multi-spectral BRDF model (ASK Model) based on the kernel-driven conception and gives an effective algorithm for broadband albedo retrieval. By adding component spectra into kernels as prior known driven variables, the new model expresses BRDF as a linear combination of wavelength-independent kernel coefficients and kernels expressed as functions of both observation geometry and wavelength. In this way, the new model brings advantages in two aspects. On the one hand, for model inversion, the new angular and spectral kernels allow combination of observations not only at different viewing and illumination angles, but also at different wavebands, which give more reliable inversion results especially when the angular data are limited. On the other hand, different from traditional narrowband-to-broadband conversion, which gives empirical weights at several available bands, the new algorithm derives broadband albedo as a weighted linear combination of kernel integrations both in angular and wavelength domains. As model validation, ground-based measurements in Heihe Field Campaign have been chosen. Results show that the new model can accurately rebuild BRDF and derive broadband albedo. Furthermore, the new model and algorithm are demonstrated using CHRIS and EOS-MODIS data. The retrieved broadband albedos have been compared with MODIS BRDF/albedo product and the *in situ* measurements. Results show that the presented algorithm can be employed to retrieve broadband albedo from multisource satellite observations.**

***Index Terms*—Albedo, bidirectional reflectance distribution function(BRDF), kernel-driven model, multi-angle, multispectra.**

NOMENCLATURE

θ_s	Solar zenith angle.
φ_s	Solar azimuth angle.
θ_v	Sensor zenith angle.
φ_v	Sensor azimuth angle.
ϕ	Relative azimuth.
λ	Wavelength.
BRDF	Bi-directional reflectance distribution function.
R	Bi-directional reflectance.
k_{geo}	Geo-optical scattering kernel.
k_{vol}	Volumetric scattering kernel.
$f_{\mathrm{iso}}\ f_{\mathrm{geo}}\ f_{\mathrm{vol}}$	Kernel coefficients of the original kernel driven BRDF model.
$C_0, \quad C_g, \quad C_v$	Kernel coefficients of ASK-1.
$c_1, \ldots, \quad c_5$	Kernel coefficients of ASK-2.
K_0	Angular and spectral Lambertian kernel.
K_{g}	Angular and spectral geo-optical kernel.
K_v	Angular and spectral volumetric kernel.
R_{multi}	Multiscattering reflectance.
$k_1, \ldots, \quad k_5$	Angular and spectral kernels in ASK-2.
a_1	Area proportion of geometrical structured surface.
a_2	Area proportion of volumetrically structured surface.
n	Density of trees.
r	Average radius of trees.
ρ_c	Leaf reflectance.
τ_c	Leaf transmittance.
ρ_g	Soil reflectance.
F	Facet number density.
ω	Single-scattering albedo.
m	Soil moisture.
A_w	Absorption factor due to the soil moisture.
$R_{i,j}^{\mathrm{obs}}$	Observed reflectance.
$R_{i,j}^{\mathrm{simu}}$	Model predicted reflectance.
W	Weighting factors.
α_{broad}	Broadband albedo.

Manuscript received June 30, 2009; revised October 31, 2009, February 02, 2010; accepted March 10, 2010. Date of publication May 24, 2010; date of current version August 25, 2010. This work was supported in part by the Chinese Natural Science Foundation Project under Contract NSFC 40730525, Contract NSFC 40701121, Contract NSFC 40871175, and Contract NSFC 40601067, by China's Special Funds for Major State Basic Research Project under Contract 2007CB714400, and by The Action Plan of Western Development of Chinese Academy of Sciences under Contract KZCX2-XB2-09.

S. Liu, Q. Liu, Q. Liu, and J. Wen are with the State Key Laboratory of Remote Sensing Science, jointly sponsored by the Institute of Remote Sensing Applications of Chinese Academy of Sciences and Beijing Normal University, Beijing 100101, China (e-mail: qhliu@irsa.ac.cn).

X. Li is with the School of Geography and Remote Sensing Science, Beijing Normal University, Beijing 100875, China.

Color versions of one or more of the figures in this paper are available online at http://ieeexplore.ieee.org.

Digital Object Identifier 10.1109/JSTARS.2010.2048745

α_λ	Spectral albedo.
G	Spectral irradiance.
α_{bb}	Broadband black-sky albedo.
α_{bw}	Broadband white-sky albedo.
α_{ba}	Broadband actual albedo.
$\alpha_{b\lambda}$	Spectral black-sky albedo.
$\alpha_{w\lambda}$	Spectral white-sky albedo.
ε_r	Relative error of actual albedo.
α_0	"True" albedo corresponding to the "ideal" dataset.
α	Inverted albedo.
$d_{0\lambda}$	Proportions of direct beam.
h_k	Directional-hemispherical integral.
H_k	Bi-hemispherical integral.
Hh_k	Combined hemispherical integral.
h_{k_new}	Broadband directional-hemispherical integral.
H_{k_new}	Broadband bi-hemispherical integral.
Hh_{k_new}	Broadband combined integral.

I. Introduction

SURFACE albedo, the hemisphere reflectivity integrated over the entire solar spectrum, is a key forcing parameter controlling the planetary radiative energy budget and the partitioning of radiative energy between the atmosphere and surface. It is a parameter needed in both global and regional climate models and is a sensitive indicator of environmental vulnerability [1]–[4]. Also, it is of critical importance in crop simulation studies because it defines how much solar radiation is available for carbon take and photolysis and ultimately effects productivity and yield [5]. It has been a challenge issue how to retrieve broadband albedo at regional and global scale with sufficient accuracy.

Albedo is dependent on the bidirectional reflectance distribution function (BRDF), which describes how the reflectance depends on view and solar angles [6]–[8]. BRDF and albedo have recently received much attention in advanced remote-sensing data analysis [9]–[11]. The Advanced Very High Resolution Radiometer (AVHRR) Polar Pathfinder group made use of STREAMER radioactive transfer model [12] and anisotropic correction factors to convert the directionally dependent top-of-the-atmosphere (TOA) reflectance to a hemispheric albedo [13]. Nevertheless, because of the deficient angular domain, a full harnessing of AVHRR data is jeopardized in many situations [14]. More accurate estimates can be obtained by inverting and then integrating mathematical BRDF models [9]–[11], [15]–[17]. In the context of having to process large number of satellite data, semiempirical models mirroring the within-land cover type surface scattering processes were first investigated more seriously in the 1990s, and now they are widely used for albedo retrieval [15], [18]. Albedo and reflectance anisotropy products from remote sensing are now routinely provided with spatial resolutions of 250 m to 20 km and temporal frequencies of daily to monthly [19]. On the one hand, albedo retrievals are based on geostationary satellite data such as Meteosat [20]–[23] and Meteosat Second Generation (MSG) [24], [25]; on the other hand, they can be retrieved from polar orbiting satellite data such as Multiangle Imaging SpectroRadiometer (MISR) [26]–[28], Clouds and the Earth s Radiant Energy System (CERES) [29], POLDER [30]–[34], Medium-Spectral Resolution, Imaging Spectrometer (MERIS) [35], and Moderate Resolution Imaging Spectroradiometer (MODIS) [36]–[38]. Their accuracy, consistency over time, and compatibility with the same or similar products from different sensors and time periods are investigated by the literature [1], [4], [19], [39], [40]. Among them, the Algorithm for MODIS Bidirectional Reflectance Anisotropy of the Land Surface (AMBRALS) which is fully developed and validated is most widely used [40]–[43]. It makes use of a semiempirical kernel-driven BRDF model and multidate, multispectral data to provide standard global 500-m and 1-km gridded and tiled products of the land surface BRDF/Albedo every eight days [15].

Currently, the albedo retrieval method first uses a BRDF model to compute narrowband albedo corresponding to the spectral band specifications of the sensor, then the narrowband albedo is converted to broadband albedo [15]. There are two shortages in this procedure. First, because satellite sensors used for the albedo retrieval carry out their measurements in discrete spectral bands, whereas the surface albedo refers to reflection of solar radiation integrated over all wavelengths (350–5000 nm), a narrowband-to-broadband conversion (NTB conversion) is indispensable which will bring extra errors [44]. The shortwave albedo is now derived from adding some converted parameters to narrowband spectral albedos confined by discrete band set of remote sensor, provided that visible and near-infrared wave bands are included [45], [46]. Second, since the inversion is against each available waveband individually by constructing functions from multi-angular observations, the result cannot be reliable unless plenty of angular distributed data are available. This is why the MODIS BRDF/ALBEDO products are currently provided with a long period of eight days. Even with such a long period to accumulate data, the quality of the retrieved albedo data is variable. Take the (MODIS albedo products (MOD43B3) in North America from 2000 to 2004 as an example: only 31.3% of pixels were retrieved with fully data-driven inversions while 13.3% did not contain any valid retrieval [47]. For climate change purposes, products are especially needed in long time series, so the consistency among products from satellite missions flown at different times are of great importance [1], [4], [19], [40], [48]. This indicates considerable potential for product improvement through the use of more reliable algorithms.

In this paper, in order to make better use of limited data, we develop a new Angular &and Spectral Kernel-driven BRDF Model (ASK Model) which can easily couple the multispectral information with multi-angular information and outline a new algorithm for broadband albedo retrieval. On one hand, the spectral and angular data are combined together to inverse a set of

kernel coefficients independent of waveband, this joint inversion will ease the dilemma of data scarcity. On the other hand, by pre-integrating kernels both in angular and spectral domain, broadband albedo can be retrieved directly from the combination of kernel coefficients and integrated kernels.

There are six main sections included: the first section gives an introduction about the development of BRDF&Albedo. In the second and third section, ASK BRDF Model and the new albedo algorithm are proposed, then model validation is given in the fourth section, after that sensitivity analysis and some issues are discussed in the fifth section, finally, conclusion is drawn in the sixth section. With various validations and sensitivity analysis at different scale, conclusions can be drawn that the model's performance is satisfactory and the retrieval results are reliable.

II. New Kernel Functions and BRDF Model

A. Introduction to Albedo and the Kernel-Driven Model for AMBRALS

Albedo is defined as the ratio of upwelling to downwelling radiative flux at the surface. Downwelling flux may be written as the sum of a collimated component and a diffuse component [7], [8]. Black-sky albedo (BSA) is defined as albedo in the absence of a diffuse component and is a function of solar zenith angle. White-sky albedo (WSA) is defined as albedo in the absence of collimated component when the diffuse component is isotropic [36]. The actual albedo derived from *in situ* measurement includes both direct beam and diffuse skylight and can be approximately expressed as a linear weighted combination of WSA and BSA [49]. The weights (proportions of direct beam $d_{0\lambda}$ and diffuse sky-light $(1-d_{0\lambda})$ are determined by aerosol parameters, such as optical depth and aerosol type. It can be obtained from field measurements or be calculated by atmospheric radiative transfer package such as 6S (Second Simulation of the Satellite Signal in the Solar Spectrum) [50].

AMBRALS expressed the BRDF as the weighted combination of kernels with incident and observed geometry as driven variables, characterizing different scattering modes [15], [51]. In AMBRALS, since the kernels are wavelength-independent, inversion of model in different waveband will result in different kernel coefficients. Basic formula of AMBRALS model can be expressed as

$$\mathrm{BRDF}(\theta_i,\theta_v,\phi,\lambda) = f_{\mathrm{iso}}(\lambda) + f_{\mathrm{geo}}(\lambda)k_{\mathrm{geo}}(\theta_i,\theta_v,\phi) + f_{\mathrm{vol}}(\lambda)k_{\mathrm{vol}}(\theta_i,\theta_v,\phi) \quad (1)$$

where $\mathrm{BRDF}(\theta_i,\theta_v,\phi,\lambda)$ stands for BRDF, $k_{\mathrm{geo}}(\theta_i,\theta_v,\phi)$ is the geo-optical scattering kernel, $k_{\mathrm{vol}}(\theta_i,\theta_v,\phi)$ is the volumetric scattering kernel, θ_i and θ_v are the zenith angles of incident and reflected light, respectively, ϕ is the relative azimuth between incident and reflected light, and $f_{\mathrm{iso}}(\lambda)$, $f_{\mathrm{geo}}(\lambda)$ and $f_{\mathrm{vol}}(\lambda)$ are kernel coefficients characterizing the proportion of the isotropic, geo-optical, and volumetric scattering part. Each kernel has explicit physical significance and stands for a typical mechanism of surface scattering [52]–[54]. For example, the RossThick and RossThin kernels represent the volumetric scattering part, the LiSparse and LiDense kernels represent the geo-optical scattering part, and the isotropic kernel represents the Lambertian reflecting part [53], [54]. Different kernel combination will be chosen in terms of the surface condition. Kernel coefficients will be derived by fitting the model to observed data. Here, the inverse wave-dependent coefficients are hard to be directly related with canopy structure parameters and the retrieved albedos are confined to narrowbands corresponding to the observed data. In former studies, empirical indexes are constructed to connect coefficients and canopy structure [55]–[57] and a process of NTB conversion is used to derive broadband albedo [45], [46].

B. Basic Form of the Kernel Functions and ASK-1 BRDF Model for Mixed Pixel

The basic form of angular and spectral kernel functions and BRDF model, namely ASK-1 BRDF model, has been developed in previous work [58]. For the convenience of the reader, we will brief the formula here. The mixed pixel is modeled as composed of two parts where the geo-optical model is applied to land covers such as sparse shrubs, trees, or crops with a soil or soil–grass understory, while the volumetric model treats canopy as homogeneous layer of isotropic oriented facets [54] Then BRDF, given as follows, can be expressed as a linear combination of these two models:

$$\mathrm{BRDF}(\theta_i,\theta_v,\phi,\lambda) = a_1\mathrm{BRDF}_{\mathrm{geo}}(\theta_i,\theta_v,\phi,\lambda) + a_2 BRDF_{\mathrm{vol}}(\theta_i,\theta_v,\phi,\lambda) \quad (2)$$

where a_1, a_2 are the weights of the two models, and they can be regarded as the area proportion of geometrical structured and volumetrically structured surface. However, in this paper, they are simply taken as semi-empirical parameters because it is difficult to divide a pixel clearly.

For the geo-optical part, the model is based on the Li and Strahler sparse canopy model [54]. It considers a plane with spheroids which is described by their density n and average radius r. $\mathrm{BRDF}_{\mathrm{geo}}(\theta_i,\theta_v,\phi,\lambda)$ is expressed as a simplified formula with two kernels and three coefficients (the third for the isotropic portion). For the volumetric scattering part, the model provided by the literature [59], [60] is used. It is for an isotropic distribution of facet slops with reflectance ρ_c and transmission τ_c above a soil reflectance of ρ_g. For this model, the facet number density and canopy height are represented by a structural constant F which is related to LAI. Here, $b = 1/2\cdot(\sec\theta_i + \sec\theta_v)$ is always approximately replaced by a constant (1.5) which is derived from averaging typical values of the angles [53]. $\mathrm{BRDF}_{\mathrm{vol}}(\theta_i,\theta_v,\phi,\lambda)$ is also expressed as a combination of two kernels and three coefficients, details for $\mathrm{BRDF}_{\mathrm{geo}}(\theta_i,\theta_v,\phi,\lambda)$ and $\mathrm{BRDF}_{\mathrm{vol}}(\theta_i,\theta_v,\phi,\lambda)$ are given as [61]

$$\mathrm{BRDF}_{\mathrm{geo}}(\theta_i,\theta_v,\phi) = b_1\cdot k^g_{\mathrm{geo}}(\theta_i,\theta_v,\phi) + b_2\cdot k^c_{\mathrm{geo}}(\theta_i,\theta_v,\phi) + b_3 \quad (3)$$

where

$$k^g_{\mathrm{geo}} = \frac{1}{\pi}(\sec\theta_i + \sec\theta_v)\cdot(t - \cos t\cdot\sin t) - \sec\theta_i - \sec\theta_r + 1$$

$$k^c_{\mathrm{geo}} = \sec\theta_i\sec\theta_v\cos^2(\xi/2) - 1$$

$$\cos t = \frac{\sqrt{D^2 + (\tan\theta_i\tan\theta_v\sin\varphi)^2}}{\sec\theta_i + \sec\theta_v}$$

$$
\begin{aligned}
D^2 &= \tan^2\theta_i + \tan^2\theta_v \\
&\quad - 2\tan\theta_i \tan\theta_v \cos\varphi \\
b_1 &= nr^2 \cdot \rho_g \\
b_2 &= \frac{2}{3} nr^2 \cdot \rho_c \\
b_3 &= \left(\frac{1}{\pi} - nr^2\right)\rho_g + \frac{2}{3} nr^2 \cdot \rho_c \\
\mathrm{BRDF}_{\mathrm{vol}}(\theta_i, \theta_v, \phi) &= d_1 \cdot k^{\rho}_{\mathrm{vol}}(\theta_i, \theta_v, \phi) \\
&\quad + d_2 \cdot k^{\tau}_{\mathrm{vol}}(\theta_i, \theta_v, \phi) + d_3
\end{aligned} \tag{4}
$$

where

$$
\begin{aligned}
k^{\rho}_{\mathrm{vol}} &= \frac{(\pi - \xi)\cos\xi + \sin\xi}{\cos\theta_i + \cos\theta_v} - \frac{\pi}{2} \\
k^{\tau}_{\mathrm{vol}} &= \frac{\xi \cdot \cos\xi + \sin\xi}{\cos\theta_i + \cos\theta_v} \\
d_1 &= \frac{2\rho_c}{3\pi^2}(1 - \exp(-bF)) \\
d_2 &= \frac{2\tau_c}{3\pi^2}(1 - \exp(-bF)) \\
d_3 &= \frac{\rho_c}{3\pi}(1 - \exp(-bF)) + \frac{\rho_g \cdot \exp(-bF)}{\pi}.
\end{aligned}
$$

In the traditional kernel-driven model, component spectra are integrated into kernel coefficients. In this paper, the component spectra are integrated into kernel functions from which the kernels are expressed as functions of both the observed geometry and wavelength, leaving the kernel coefficients universal for all bands. After substituting (3) (4) into (2) and rearranging the polynomial, the ASK-1 model can be derived as

$$
\begin{aligned}
&\mathrm{BRDF}(\theta_i, \theta_v, \phi, \lambda) \\
&\quad = C_0 K_0(\lambda) + C_{\mathrm{g}} K_{\mathrm{g}}(\theta_i, \theta_v, \phi, \lambda) + C_v K_v(\theta_i, \theta_v, \phi, \lambda)
\end{aligned} \tag{5}
$$

where

$$
\begin{aligned}
K_0(\lambda) &= \frac{\rho_g}{\pi} \\
K_g(\theta_i, \theta_i, \phi, \lambda) &= \frac{2}{3\pi}\rho_c\left(k^{c}_{\mathrm{geo}} + 1\right) + \frac{\rho_g}{\pi} \cdot k^{g}_{\mathrm{geo}} \\
K_v(\theta_i, \theta_i, \phi, \lambda) &= \frac{2\rho_c}{3\pi^2} k^{\rho}_{\mathrm{vol}} + \frac{2\tau_c}{3\pi^2} k^{\tau}_{\mathrm{vol}} + \frac{\rho_c}{3\pi} \\
C_0 &= a_1 \cdot (1 - n\pi r^2) + a_2 \cdot \exp(-bF) \\
C_g &= a_1 \cdot n\pi r^2 \\
C_v &= a_2 \cdot (1 - \exp(-bF)).
\end{aligned}
$$

In this model, the first term as function of soil reflectance represents the Lambertian reflecting part from the ground. The second term expressed as a function of the original geo-optical kernels and component spectra is applied to describe the geo-optical reflecting part. Similarly, the third part represents the volumetric scattering part.

Here, C_0, C_g, C_v are kernel coefficients stand for the weights of different scattering parts. They are all independent from wavelength and related to the structure of canopy or mixed pixel. Although all of the kernel coefficients have clear physical meaning, they can also be treated as empirical parameters, given the semi-empirical nature of kernel-driven models. $K_0(\lambda), K_{\mathrm{g}}(\theta_i, \theta_v, \phi, \lambda), K_v(\theta_i, \theta_v, \phi, \lambda)$ are angular and spectral kernels considered as known functions, with component spectra given typical values acquired from *a priori* knowledge database.

Like any other model of the same vein, ASK is semi-empirical in nature and several implications should be pointed out. First, some variables in ASK model are empirical and their physical significance can not be specifically defined. For example, F is not equal to LAI (leaf area index), although these two variables are closely related. Second, ASK can not be operated forwardly because some input variables can not be measured independently, e.g., a_1, a_2 and F. The main objective of ASK is to be used in inverse mode to estimate a set of parameters that best characterize the angular and spectral feature of land surface BRDF and enable convenient retrieval of albedo.

C. Consideration of Multiple Scattering and Soil Spectral Variation

1) Correction for Multiple Scattering: ASK-1 model is constructed on formulas from former literatures on kernel-driven model, in which simplifications have been made to the geo-optical scattering and volumetric scattering process. Most of the simplifications are acceptable tradeoffs for an empirical model, but there are also several simplifications that should be reconsidered when component spectra are into kernel functions.

An issue requiring more attention is the impact of multiple scattering between soil and vegetation [14]. The volumetric kernel provided by the literature [60] neglects the contribution from multiple scattering. It is acceptable in former applications because the multiple scattering effects can be partly represented by the isotropic kernel and physical meaning of isotropic kernel coefficient is not required. However, in the new angular and spectral model, we need to derive consistent formula for both the visible band, where multiple scattering is not significant, and the near-infrared band, where multiple scattering is dominant; ignoring the multiple scattering is in no way compensatable. In this paper, we revise the volumetric kernel by adding the multiple scattering term proposed by the literature [62]. It expresses bidirectional reflectance of a semi-infinite medium as a sum of single-scattered r_{sin} and multiscattered part r_{multi}. From the resulting expression, the following term is added to volumetric kernel as a correction for multiscattering:

$$
r_{\mathrm{multi}} = \frac{1 - \sqrt{1 - \omega}}{1 + 2\cos(\theta_i)\sqrt{1 - \omega}} \tag{6}
$$

where ω is the single-scattering albedo. Although it is not directly measurable with a device, it can always be approximately expressed as $\omega = \rho_c + \tau_c$.

2) Involving Soil-Moisture for Soil Reflectance: In our sensitivity analysis of model parameters, soil reflectance ρ_g illustrates the highest sensitivity and shows the strongest correlation to the canopy reflectance under the sparse assumption. Because of the significant variation in reflectance of soil, it should be treated as an unknown variable instead of being given typical values. There are many factors influence soil spectral. For a certain pixel in earth surface, some of the soil properties, such soil type, color, roughness, have less temporal changes and are possible to be stored in knowledge database, while other properties, such as moisture, are more unpredictable and can not be treated as constant. In this paper, we will assume the uncertainty of soil spectrum comes from its unknown moisture. According to the

study of [63], there exists an exponential relationship between soil moisture in and soil reflectance

$$\rho_g(m,\lambda) = \rho_g(0,\lambda)\cdot\exp(-A_w(\lambda)\cdot m) \tag{7}$$

where $\rho_g(m,\lambda)$ is the reflectance of the wet soil in the spectral band λ, $A_w(\lambda)$ is the absorption factor in the spectral band λ due to soil moisture m, and $\rho_g(0,\lambda)$ is the theoretical reflectance of the soils with a soil water content at air dryness. In this paper, first-order approximation of (7) is made near a reference value of soil moisture m_0

$$\rho_g(m,\lambda) = \rho_g(m_0,\lambda) - \rho_g(m_0,\lambda)\cdot A_w(\lambda)\cdot(m-m_0) \tag{8}$$

where m_0 is the value of soil moisture corresponding to the state when soil reflectance $\rho_g(m_0,\lambda)$ was collected into *a priori* knowledge database. The geometric and volumetric part in a mixed pixel can be of different soil moisture.

3) Final Form of the Kernel Functions and BRDF Model: By adding (6) into volumetric scattering model and substituting $\rho_g(\lambda)$ with $\rho_g(m,\lambda)$, the revised kernel model becomes

$$\begin{aligned} &R(\theta_i,\theta_v,\phi,\lambda)\\ &\quad= \mathrm{c}_1\cdot k_1(\lambda) + c_2\cdot k_2(\lambda) + c_3\cdot k_3(\theta_i,\theta_v,\phi,\lambda)\\ &\quad+ c_4\cdot k_4(\theta_i,\theta_v,\phi,\lambda) + c_5\cdot k_5(\theta_i,\theta_v,\phi,\lambda) \end{aligned} \tag{9}$$

where

$$\begin{aligned} k_1(\lambda) &= \frac{\rho_g(m_0,\lambda)}{\pi}\\ k_2(\lambda) &= -\frac{A_w(\lambda)\cdot\rho_g(m_0,\lambda)}{\pi}\\ k_3(\theta_i,\theta_v,\phi,\lambda) &= \frac{2}{3\pi}\rho_c(\lambda)\cdot\left(k^c_{\mathrm{geo}}+1\right)\\ &\quad+\frac{1}{\pi}k^g_{\mathrm{geo}}\cdot\rho_g(m_0,\lambda)\\ k_4(\theta_i,\theta_v,\phi,\lambda) &= -\frac{1}{\pi}k^g_{\mathrm{geo}}\cdot A_w(\lambda)\cdot\rho_g(m_0,\lambda)\\ k_5(\theta_i,\theta_v,\phi,\lambda) &= \frac{2}{3\pi^2}\rho_c(\lambda)\cdot k^\rho_{\mathrm{vol}}\\ &\quad+\frac{2}{3\pi^2}\tau_c(\lambda)\cdot k^\tau_{\mathrm{vol}}+\frac{1}{3\pi}\rho_c(\lambda)\\ &\quad+\frac{1-\sqrt{1-\omega(\lambda)}}{\pi(1+2\cos(\theta_i)\sqrt{1-\omega(\lambda)})}\\ c_1 &= a_1\cdot(1-n\pi r^2)+a_2\cdot\exp(-bF)\\ c_2 &= a_1\cdot(1-n\pi r^2)\cdot(m_1-m_0)\\ &\quad+a_2\cdot\exp(-bF)\cdot(m_2-m_0)\\ c_3 &= a_1\cdot n\pi r^2\\ c_4 &= a_1\cdot n\pi r^2\cdot(m_1-m_0)\\ c_5 &= a_2\cdot(1-\exp(-bF)). \end{aligned}$$

Like ASK-1, the kernels are functions of sun/view angles and component spectra; and kernel coefficients are wavelength-independent One may observe that c_1, c_3, c_5 are much alike C_0, C_g, C_v in (5) in their formula. However, we emphasize that this model should be treated as more empirical than strictly physical, and the kernel coefficients are simply the result of fitting observation. So we will denote them with different symbols to avoid confusion. In Section III, the final form (9) of ASK model will be addressed as "ASK-2."

III. Model parameters Inversion and Albedo Retrieval

A. Model Inversion

BRDF is expanded into a linear sum of kernels. This allows the flexibility and efficiency for bidirectional reflectance inversion and albedo computation be programmed in kernel-oriented, rather than model-oriented, fashion. Under the assumption that the spectral variables related to characteristic of land surface are designated with prior known typical values, all kernels' values occurring at the viewing and illumination angles at hand can be computed in advance and tabulated so that the functions only need to be processed once for each geometric situation and every single kernel which allows both rapid computation and free combination of any number of kernels.

In ASK-2, we will treat $c_1,\ldots,c_5$ as unknown variables. $M\times N$ equations are constructed for M-band and N-band observations from satellite image corrected with atmospheric effects or *in situ* measurements. In the inversion process, the unknown variables are determined in the context of least-square error fitting, i.e., through minimization of a cost function, as

$$\mathrm{COST} = \sum_{i=1}^{M}\sum_{j=1}^{N}\frac{\left(R^{\mathrm{obs}}_{i,j}-R^{\mathrm{simu}}_{i,j}\right)^2}{W_i\cdot W_j} \tag{10}$$

where M is the number of observations, N is the number of wave bands involved in the inversion, $R^{\mathrm{obs}}_{i,j}$ and $R^{\mathrm{simu}}_{i,j}$ refer to the observed and model predicted reflectance for a given set of geometric angles (θ_i,θ_v,ϕ), respectively, and W_i and W_j are weighting factors that could reflect different weights assigned to different observations and bands if desired. For example, in this paper, the weights for data in different MODIS bands are proportional in ratio to the nominal spectral radiance given in the MODIS bands specification, i.e., [21.8, 24.7, 35.3, 29.0, 5.4, 7.3, 1] for band 1 to band 7, and weights for different observations are constant. Since there are five unknown variables and their corresponding kernel functions are not orthogonal, it is possible that the inversion will over fit the data and become unstable. To avoid undesirable inversion result, boundary limitations to the unknown variables are designated at first. Considering their physical meaning, c_1, c_3, and c_5 are restricted to [0, 1] while c_2 and c_4 are restricted to $[-0.5, 0.5]$. Besides solid boundary, soft constraints such as Bayes constraint are also common resort to stabilize the multivariant inversion. Since k_2 and k_4 are additional terms related to difference of soil spectra between real scene and that prior given in ASK-2, in order to lower the influence from the soil background, Here, a term $c_2^2+c_4^2$ is also added into the cost function as soft constraint and give it a very small constant weight. As we known, k_2 and k_4 are related to difference between soil spectra of real scene and that of *a priori* value, and the fail-safe value for c_2 and c_4 should be 0. So, this soft constraint will ensure that c_2 and c_4 go to fail-safe value in ill-posed situation, i.e., the information in observations is not enough to invert all 5 unknowns; for normal situations, the influence of this term on the model's fitting ability is negligible because the weight is slight.

The inversion of ASK-1 model is similar, except that the boundary restrictions are assigned with $[0, \inf]$ for C_0, C_g and C_v. As described before, the ASK model is used as semi-empirical model. Under the circumstance that the inversion is stable, allowing the variables to take value in a wider range would increase the fitting ability of the model.

As a linear model, the ASK BRDF model can be inverted analytically by matrix inversion [64], which avoids costly numerical inversion problems arising in the physical models and gives much more reliable and robust results than the empirical ones.

B. Retrieval of Spectral Albedo

In order to retrieve spectral albedo, the directional-hemispherical integral $h_k(\theta_i, \lambda)$ and bi-hemispherical integral $H_k(\lambda)$ of the kernel functions are defined as in (14)–(15). Benefiting from the linear characteristics, spectral black-sky albedo $H_k(\lambda)$ and spectral white-sky albedo $\alpha_{w\lambda}$ can be derived as a weighted combination of $h_k(\theta_i, \lambda)$ and $H_k(\lambda)$ separately. Then spectral actual albedo $\alpha_{a\lambda}(\theta_i)$ can be derived from combination of $\alpha_{b\lambda}(\theta_i)$ and $\alpha_{w\lambda}$ weighted by $d_{0\lambda}$ and $1 - d_{0\lambda}$. Similarly, $Hh_k(\theta_i, \lambda)$ is defined as given in (16), and then $\alpha_{a\lambda}(\theta_i)$ is the combination of $Hh_k(\theta_i, \lambda)$ weighted by c_k. Since the suite of kernels shared the same angle-related formula, this makes the code efficient by avoiding duplication of computations for kernel integration [23]:

$$\alpha_{b\lambda}(\theta_i) = \sum_k c_k h_k(\theta_i, \lambda) \tag{11}$$

$$\alpha_{w\lambda} = \sum_k c_k H_k(\lambda) \tag{12}$$

$$\alpha_{a\lambda} = \sum_k c_k Hh_k(\theta_i, \lambda) \tag{13}$$

$$h_k(\theta_i, \lambda) = \frac{1}{\pi} \int_0^{2\pi} \int_0^{\frac{\pi}{2}} [K_k(\theta_i, \theta_v, \psi, \lambda)] \times \sin\theta_v \cos\theta_v d\theta_v d\psi \tag{14}$$

$$H_k(\lambda) = 2 \int_0^{\frac{\pi}{2}} h_k(\theta_i, \lambda) \sin\theta_i \cos\theta_i d\theta_i \tag{15}$$

$$Hh_k(\theta_i, \lambda) = d_0 h_k(\theta_i, \lambda) + (1 - d_0) H_k(\lambda). \tag{16}$$

C. Spectral-to-Broadband Albedo Conversion

In practice, the total energy reflected by the Earth's surface in the shortwave domain is characterized by the shortwave (0.3–5.0 μm) broadband albedo defined as the ratio of broadband upwelling radiative flux to broadband downwelling flux. Frequently, the visible (0.3–0.7 μm) and near-infrared (0.7–1.3 μm) broadband albedos are also of interest due to the marked difference of the reflectance of vegetation in these two spectral regions [36]. Therefore, a conversion process from spectral to broadband albedo is necessary.

Starting from the definition, broadband albedo can be related to spectral albedo through spectral integration weighted by the bottom-of-atmosphere downwelling spectral solar flux. Hence, provided we know the spectral albedo α_λ and the incident spectral irradiance $G(\lambda)$, the conversion equation reads as

$$\alpha_{\text{broad}} = \frac{\int_{\lambda_1}^{\lambda_2} G(\lambda)\alpha_\lambda d\lambda}{\int_{\lambda_1}^{\lambda_2} G(\lambda) d\lambda} = \int_{\lambda_1}^{\lambda_2} w_\lambda \alpha_\lambda d\lambda$$

$$w_\lambda = \frac{G(\lambda)}{\int_{\lambda_1}^{\lambda_2} G(\lambda) d\lambda}. \tag{17}$$

Here, α_{broad} is broadband albedo of the surface with spectral range from λ_1 to λ_2, α_λ is the spectral albedo, and $G(\lambda)$ is the spectral incident irradiance.

Since the satellite sensors carry out their measurements in several narrowbands, the inversed wavelength-dependent kernel coefficients are confined to these specific wavebands in former studies of computing albedo from kernel-driven BRDF model. It limits the ability of deriving broadband albedo directly from

$$\begin{aligned}\alpha_{\text{bb}}(\theta_i) &= \int_{\lambda_1}^{\lambda_2} w_\lambda \alpha_{b\lambda}(\theta_i) d\lambda \\ &= \sum_k c_k \cdot \int_{\lambda_1}^{\lambda_2} w_\lambda h_k(\theta_i, \lambda) d\lambda \\ &= \sum_k c_k \cdot h_{k\_\text{new}}(\theta_i)\end{aligned} \tag{18}$$

$$\begin{aligned}\alpha_{\text{bw}} &= \int_{\lambda_1}^{\lambda_2} w_\lambda \alpha_{w\lambda} d\lambda \\ &= \sum_k c_k \cdot \int_{\lambda_1}^{\lambda_2} w_\lambda H_k(\lambda) d\lambda \\ &= \sum_k c_k \cdot H_{k\_\text{new}}\end{aligned} \tag{19}$$

$$\begin{aligned}\alpha_{\text{ba}}(\theta_i) &= \int_{\lambda_1}^{\lambda_2} w_\lambda \alpha_{a\lambda} d\lambda \\ &= \sum_k c_k \cdot \int_{\lambda_1}^{\lambda_2} w_\lambda Hh_k(\theta_i, \lambda) d\lambda \\ &= \sum_k c_k \cdot Hh_{k\_\text{new}}(\theta_i)\end{aligned} \tag{20}$$

when the number of bands are not sufficient enough. Prior attempts in converting narrowband albedo to broadband focused on establishing empirical equations by model simulation under general atmospheric conditions with respect to different sensors [2], [45], [65], [66]. Beyond arising extra errors, the conversion is in different manner with respect to surface characteristic, atmosphere state and remote sensors. Obviously, it is difficult to be put into general applications.

In this study, the wave-independent kernel coefficients enable a handy way out of the dilemma of narrowband-to-broadband albedo conversion. Different from the original algorithm, the kernels here are integrated not only at angle dimension but also at wavelength dimension as shown in

$$h_{k\_\text{new}}(\theta_i) = \int_{\lambda_1}^{\lambda_2} w_\lambda h_k(\theta_i, \lambda) d\lambda \tag{21}$$

$$H_{k\_\text{new}} = \int_{\lambda_1}^{\lambda_2} w_\lambda H_k(\lambda) d\lambda \tag{22}$$

$$Hh_{k\_\text{new}}(\theta_i) = \int_{\lambda_1}^{\lambda_2} w_\lambda Hh_k(\theta_i, \lambda) d\lambda. \tag{23}$$

This step can be achieved by assigning w_λ and other spectral related variables with prior known values according to atmosphere state and surface component characteristics. Through this process, the broadband black-sky, white-sky and actual

albedo $\alpha_{\rm bb}(\theta_i), \alpha_{\rm bw}, \alpha_{\rm ba}(\theta_i)$ can be respectively expressed as a linear weighted combination of new integral kernels $h_{k\_\rm new}(\theta_i), H_{k\_\rm new}, Hh_{k\_\rm new}(\theta_i)$, where the weights c_k are the same as those inverted from ASK BRDF Model [see (18)–(23)]. Note that $h_{k\_\rm new}(\theta_i), H_{k\_\rm new}$ and $Hh_{k\_\rm new}(\theta_i)$ are dependent on neither the observations nor wavelength and could therefore be tabulated as functions of atmosphere state and surface component characteristics, the spectral BSA at any solar zenith angle and spectral WSA can be constructed directly from the inversed kernel coefficients and integrals from lookup tables (LUTs). Broadband albedo can be derived by integrating continuous spectral albedos with spectral resolution as fine as component spectra. Obviously, the conversion process is based on mathematical method and can be universally applicable for different data source with respect to sensors and platforms.

IV. Validation

Validation of the BRDF/Albedo derived from the proposed model will be performed in three aspects. Meanwhile, the results of ASK are compared with its predecessors RossLi which is employed in AMBRALS. First, the model needs to be validated for as many types of land cover as possible to ensure that it provides adequate mathematical description of BRDF shapes. This is done by using both field-measured and spaceborne multi-angular observations. Second, the retrieved albedos will be compared with *in situ* measured albedos. Third, as a demonstration, the new albedo algorithm will be applied to CHRIS and MODIS images with fine and coarse resolution respectively, to investigate its performance on pure and mixed pixels. Results will also be compared to MODIS albedo product.

Model validation is based on dataset of the Watershed Airborne Telemetry Experimental Research (WATER Experiment). Field measurements were performed around the suburb of Zhangye city, Gansu province, in the middle reaches of the Heihe River Basin during May–July 2008. The central geographic location is 38.86N, 100.41E. Most measurements were made separately at five sites within a perimeter of 10 km around this central location. Meanwhile, airborne and spaceborne data with different temporal and spatial resolution are collected during the experiment. In this study, observations from multi-angular observing sensor CHRIS/PROBA, as well as MODIS daily reflectance (MOD09) products and eight-day surface albedo (MCD43A3) products collected during the campaign were used.

A. Ability of the Kernel Functions to Fit BRF Data

1) Fitting Field-Measured BRF (Pure Pixel): ASK BRDF model targets on applications at the global scale. It is designed to describe the bidirectional reflectance of mixed land cover types. But before measurements for heterogeneous scenes are available, it is necessary and useful to validate the model using field-measured data over a single land cover type. Then it can be expected that the model will display its strength more obviously for mixed pixels [67]. Thus, the ASK BRDF model is first tested with *in situ* collection of measurements. Field measurements for our validation purpose are multi-angular reflectance spectra of a variety of surface cover types including crops, semi-desert and natural plants. Hemispheric-conical reflectance factor (HCRF) data have been acquired from 350 to 2500 nm using ASD spectrometer with a field-of-view of 25° mounted on a portable multi-angular observation. For wheat and corn, the target was viewed under 48 view directions distributed every 5° interval for zenith angle θ_v in four different azimuthally planes, namely, principle plane, perpendicular plane, along row plane and across row plane. For semi-desert shrub and bulrush data set, the latter two viewing plane are disregarded because the plants were distributed randomly without row structure. In this research, the measured HCRF is used as bidirectional reflectance factor (BRF) despite they are differently defined by the literature [7], [8]. This approximation will not seriously disturb the BRDF/Albedo retrieval because ASK Model is semiempirical itself.

TABLE I
Wavelength for MODIS Bands 1–7

MODIS	B1	B2	B3	B4	B5	B6	B7
Wavelength (nm)	620 -670	841 -876	459 -479	545 -565	1230 -1250	1628 -1652	2105 -2155

Six sets of *in situ* measurements are chosen to validate ASK model: corn data measured in both May 30th and July 1st at Yingke experiment field 1; wheat data measured in June 9th at Yingke experiment field 2; semi-desert data collected in June 14th in Huazhaizi semi-desert experiment field; bulrush and clover data acquired in June 26th near Linze Grassland station. In turn, we define them as datasets 1–6 in the following tables and figures. Both canopy and component spectral measurements are convolved into MODIS wavebands listed in Table I according to the MODIS band response functions, and data of the first seven spectral bands are used in model inversion given the weights mentioned in Section III-A.

In this study, the fixed leaf spectra and soil reflectance are from field measurement during the experiment, while soil moisture attenuating factor are from former laboratory experiment [68]. Since this model is semi-empirical itself, using the typical data taken from literature or other measured dataset will not bring too much error. ASK-2 model is expected to perform better than ASK-1 with respect of both fitting ability and soundness of model parameters, so for the rest of this paper, we will focus our analysis on ASK-2 model.

Table II shows the model-fitting relative root mean square error (R-RMSE) defined as the RMSE divided by angular average BRF of ASK-2 for the six BRF datasets in the seven MODIS bands. Even though there are some deviations, the R-RMSEs are always below 0.2 except several abrupt values. The model's worst performance occurs in semi-desert dataset for which the inversed coefficient c_1 reaches its upper limit and the other four are all close to 0. This is due to the scene of semi-desert is almost bare and greatly deviate from the model assumption on soil-vegetation system. When the ASK Model is applied in such case, the input component spectral especially the soil spectra must be chosen carefully.

Table III gives the R-RMSE of traditional kernel driven BRDF model (RossLi model) for which the inversion is conduct separately for each MODIS waveband. Comparing Table II with Table III, it can be observed that ASK-2 shows similar fitting ability with RossLi model in bands 1–4 but larger R-RMSE for bands 5–7. This is because of the smaller weights

TABLE II
FITTING R-RMSE OF ASK-2 IN MODIS BANDS 1–7

	B1	B2	B3	B4	B5	B6	B7	obs.
1	0.081	0.047	0.128	0.087	0.144	0.270	0.394	48
2	0.215	0.073	0.713	0.138	0.167	0.376	0.295	56
3	0.238	0.055	0.190	0.154	0.257	0.462	0.307	47
4	0.120	0.071	0.114	0.122	0.054	0.056	0.099	28
5	0.216	0.153	0.291	0.238	0.203	0.409	0.507	54
6	0.332	0.064	0.345	0.177	0.188	0.458	0.333	42

TABLE III
FITTING R-RMSE OF ROSSLI KERNEL DRIVEN MODEL IN MODIS BANDS 1–7

	B1	B2	B3	B4	B5	B6	B7
1	0.123	0.053	0.132	0.109	0.065	0.083	0.112
2	0.137	0.038	0.114	0.068	0.035	0.034	0.088
3	0.272	0.044	0.255	0.206	0.062	0.139	0.270
4	0.050	0.038	0.053	0.049	0.032	0.036	0.067
5	0.106	0.100	0.102	0.082	0.088	0.084	0.108
6	0.067	0.052	0.078	0.065	0.045	0.051	0.113

given to bands 5–7 in the wave-joint inversion of ASK-2. It is theoretically reasonable that wave-separate inversion fit data better than wave-joint inversion. Even though ASK-2 sacrifices some fitting ability in order to achieve more stability, these bigger fitting residuals occur in wavebands that are less significant to the retrieval of broadband albedo. Another thing should be pointed out is that ASK-2 is still feasible when inversion of RossLi fail due to the limited observations.

Table IV lists the inverted kernel coefficients of ASK-2 for the six BRF datasets. In ASK-2, since c_1, c_3, and c_5 represent weights of background, geometric scattering, and volumetric scattering respectively, their values should have the ability to indicate the scene configuration. It can be seen from Table IV that c_1 is close to 1 for corn-20080530 and desert datasets while there is little vegetation; it is close to 0 for corn-20080701 and clover datasets while there is almost full vegetation cover. The volumetric scattering part c_5, exhibits large values in the clover, corn-20080701 and bulrush datasets, and decreases for other datasets of less vegetation. The geometric scattering part c_3 is also explainable: its large value occurs at corn-20080530 dataset which is kind of discrete and sparse vegetation; also at wheat dataset which is of row structure and clover dataset which shows distinct clustering. Parameters c_2 and c_4 are linked to soil moisture. Positive values of c_2 and c_4 for corn-20080701 and clover datasets indicate that the soil background of these datasets are wetter than the reference value; while negative value of c_2 for desert dataset indicates that soil in desert is dryer than the reference. As authors of this paper participated in the experiment, it is convinced that the judgments above agree with the experiences in field experiment.

2) Fitting Satellite Measured BRF (Mixed Pixel): In order to test ASK model's fitting ability for mixed pixel at regional scale. High-quality cloud-cleared and atmospherically corrected MODIS daily reflectance product (MOD09) was

TABLE IV
INVERSE COEFFICIENTS OF ASK-2 FOR THE SIX BRF DATASETS

	c_1	c_2	c_3	c_4	c_5
1	0.95047	-0.00061	0.29146	-0.00274	0.00000
2	0.00000	0.00755	0.09170	0.00088	0.68431
3	0.19070	-0.00036	0.23586	-0.00001	0.43965
4	1.00000	-0.02885	0.03330	0.00359	0.03107
5	0.00110	0.00023	0.06108	0.00564	0.56582
6	0.00000	0.00647	0.14885	0.00238	0.78965

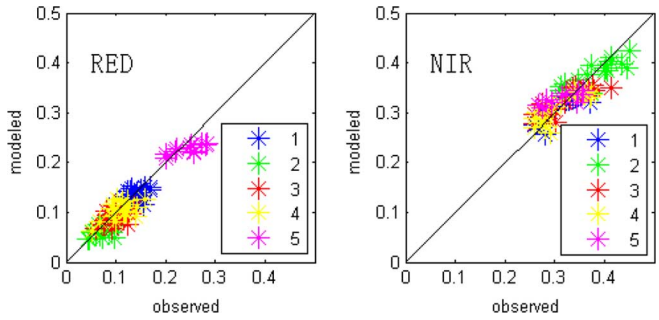

Fig. 1. Modeled and observed BRF from 16-day period MOD09.

TABLE V
FITTING R-RMSE OF ASK-2 FOR THE MOD09 WITH 16-DAY PERIOD

	B1	B2	B4	B5	B6	B7	obs.
1	0.120	0.056	0.090	0.063	0.101	0.148	20
2	0.241	0.071	0.140	0.089	0.177	0.156	18
3	0.202	0.082	0.142	0.111	0.146	0.178	17
4	0.116	0.083	0.113	0.092	0.074	0.122	11
5	0.163	0.086	0.139	0.075	0.170	0.428	14

collected over a 16-day period corresponding to each *in situ* measurement. The cloud contaminated products are screened out according to the accompanied QA flag associated with each pixel. In the inversion process, the first seven bands except the B3, which is strongly contaminated by atmosphere, are employed to present multispectral information while either 5-day or 16-day period accumulation around the date of *in situ* measurement is used to construct multi-angular datasets. For example, for *in situ* measurement of corn-080530, DOY (day of year) 151, MOD09 data are collected within DOY 144–159 and DOY 149–153, respectively, for a 16-day and 5-day period. Fig. 1 compares the modeled BRF with the observed ones from MOD09 at Red & NIR band separately for each surface type. The R-RMSEs listed in Table V are found to be smaller than that for the inversion against field measurements, indicating that the ASK model is of better fitting ability for regional than local scale observations, for mixed pixel than pure pixel. This is reasonable as for pure pixels, either geometric or volumetric scattering dominates which will lead to too large or too small weights, while for mixed pixels these two types coexist and more balanced weights will be derived. This is just where the ASK model shows its advantage as a compromise of geo-optical and radiative transfer BRDF models.

TABLE VI
INVERSE COEFFICIENTS OF ASK-2 FOR THE MOD09 WITH 16-DAY PERIOD

	c_1	c_2	c_3	c_4	c_5
1	0.682275	-0.000550	0.261041	0.006645	0.111087
2	0.184888	-0.000570	0.208922	0.008401	0.441636
3	0.441150	-0.000460	0.316158	0.005385	0.219601
4	1.000000	-0.026790	0.139621	-0.005840	0.000000
5	0.678888	-0.001080	0.318310	0.015694	0.128207

B. Applicability of Using Angular and Spectral Kernel Functions to Calculate Albedo

1) Albedo Validation With Field Measurements: In Table VII, modeled shortwave (0.3–5.0 μm) broadband albedos derived from the new algorithm are compared with both the retrievals of RossLi BRDF model and the simultaneously *in situ* measurements of albedometer. The inversion is performed using field-measured BRF and MOD09 products as described in Section IV-A, so the inverse coefficients from Table IV and Table VI are directly used to retrieve albedos in this part. *in situ* measurements of albedo were made in two different ways. One was from two albedometers mounted on a 10-m tower in an automatic weather station (AWS) near the center of the study area. These measurements are recorded based on a 10 minutes average. Other measurements were made from two additional albedometers mounted at the top of a tripod (about 1.5 m high). These portable albedometers record albedo at 5-min intervals without average and could be moved from one place to another, usually placed in similar cover type as that of BRF measurement. As for the broadband albedo retrieval for RossLi, we used the method in AMBRALS [38], [65]. Additionally, the visible (0.3–0.7 μm) (VIS) and near-infrared (0.7–1.3 μm) (NIR) broadband albedos are also retrieved with field BRF and Mod09 16-day and 5-day observation for ASK-2 and RossLi. Results and comparisons are given in Tables VIII and IX.

Table VII lists the retrieved shortwave albedo and *in situ* measurements for different surface types. It is obvious that the retrievals from field-measured BRF data of ASK-2 are in better agreement with albedometers measurements compared with its predecessor RossLi. Results of ASK-2 are satisfactory except for the second dataset of corn-20080701 whose retrievals are much higher than the AWS records. This may be attributed to the distance between the AWS and the place of BRF measurements, and the irrigation pattern that caused a heterogeneous distribution in soil moisture. In comparison, the albedo retrieved from MOD09 data deviate more from albedometer measurements, which can be easily explained by the scale mismatch between the *in situ* and spaceborne observations. In this research, the field measured albedos are for homogeneous land cover in a circle area with radius of several meters, while the MODIS observations are based on 500-m resolution and different land cover types are usually included in one pixel. This finding coincides with some former studies which indicated the inability of directly validating retrieved albedo at regional scale with field measured albedos [41] More investigation is needed, and we will discuss this issue in the next section.

2) Algorithm Demonstration on Satellite Images: For regional-scale validation, operation of ASK-2 model on three MOD09 datasets is demonstrated composed of 16 day-period starting from DOY145 (from May 25th, 2008, to June 10th, 2008), DOY153 and DOY161 respectively, corresponding to the MODIS albedo product (MOD43A3). In addition, we also construct another MOD09 dataset starting from DOY154 to DOY169 centered on June 4th, 2008, which aims at comparison with CHRIS retrievals. Considering the atmosphere correction problem, the third band is excluded in the inversion

TABLE VII
ACTUAL SHORTWAVE ALBEDO OF ASK-2/ROSSLI RETRIEVAL AND ALBEDEMETER MEASUREMENT

		Actual shortwave Albedo				
		Field	16-day	5-day	AWS*	OBS**
1	ASK-2	0.1677	0.1681	0.1738	0.1683	0.183
	RossLi	0.2141	0.1852	0.1888		
2	ASK-2	0.1802	0.1687	0.1791	0.1489	***
	RossLi	0.1955	0.1989	0.1772		
3	ASK-2	0.1455	0.1411	0.1736	***	0.1434
	RossLi	0.1824	0.1928	0.1894		
4	ASK-2	0.2649	0.2207	0.1956	0.2498	0.2348
	RossLi	0.2668	0.2674	0.3092		
5	ASK-2	0.1734	0.1901	0.2087	***	***
	RossLi	0.2045	0.2239	0.2039		
6	ASK-2	0.2261	***	***	***	***
	RossLi	0.2391	***	***		

* AWS denotes albedometer measurements from automatic weather station
** OBS denotes portable albedometer measurements
*** albedemeter measurements are not available for some targets; and the fields of clover and bulrush fall in the same pixel in MODIS image.

TABLE VIII
ACTUAL VIS BROADBAND ALBEDO OF ASK-2&ROSSLI

	Field		16-day		5-day	
	ASK-2	RossLi	ASK-2	RossLi	ASK-2	RossLi
1	0.0632	0.1382	0.0801	0.0961	0.0837	0.0960
2	0.0397	0.0364	0.0452	0.0648	0.0522	0.0606
3	0.0177	0.0596	0.0432	0.0872	0.0631	0.0793
4	0.1787	0.1986	0.1410	0.1711	0.1269	0.2084
5	0.0552	0.0615	0.0884	0.1172	0.0971	0.0954
6	0.0415	0.0592	***	***	***	***

TABLE IX
ACTUAL NIR BROADBAND ALBEDO OF ASK-2&ROSSLI

	Field		16-day		5-day	
	ASK-2	RossLi	ASK-2	RossLi	ASK-2	RossLi
1	0.2288	0.3031	0.2586	0.2781	0.2664	0.2832
2	0.3716	0.3560	0.2942	0.3272	0.3081	0.2855
3	0.2866	0.3031	0.2407	0.3102	0.2862	0.3051
4	0.3628	0.3484	0.3040	0.3726	0.2675	0.4153
5	0.3436	0.3604	0.2944	0.3301	0.3231	0.2954
6	0.4367	0.4153	***	***	***	***

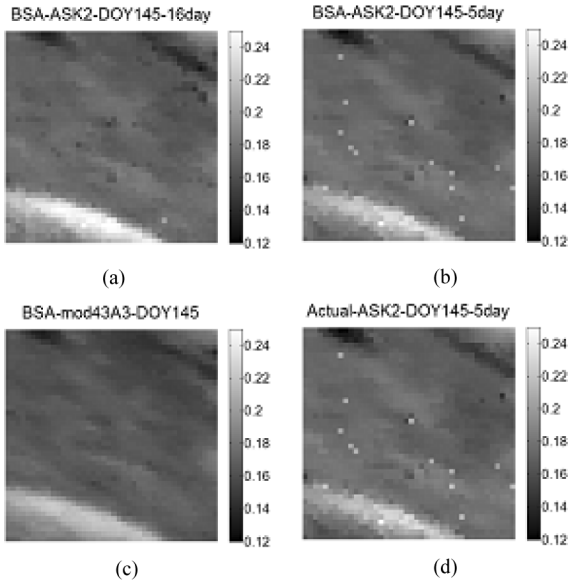

Fig. 2. ASK-2 retrieval (BSA and Actual Albedo) from (a), (b), (d) MOD09 versus (c) MOD43A3 for DOY145.

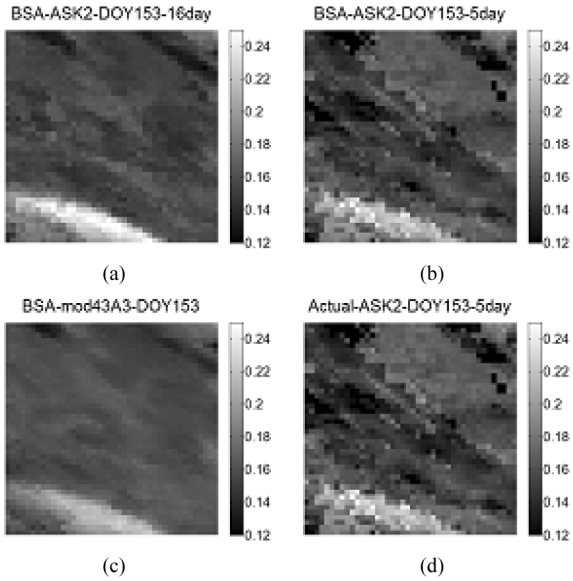

Fig. 3. ASK-2 retrieval (BSA and Actual Albedo) from (a), (b), (d) MOD09 versus (c) MOD43A3 for DOY153.

process. With 500-m spatial resolution, 42×42 pixels centered in Yingke experiment site are selected to derive black-sky shortwave albedo and white-sky shortwave albedo. Figs. 2–4 illustrate that the BSA retrievals based on the 16-day period from ASK-2 generally agree with MOD43A3 for all three datasets. As for the retrievals based on a 5-day period on the right, some pixels of the second and third datasets seem darker than their counterparts on the left image. The difference is reasonable because 16 days is not a sufficiently short period to assure the unchanged surface state, especially for cropland in the specific growth stage. Additionally, there are several times of irrigation after June 3rd, 2008, during the period on the different cropland plot each time, which will largely affect the reflecting property of surface and lower the albedo. This

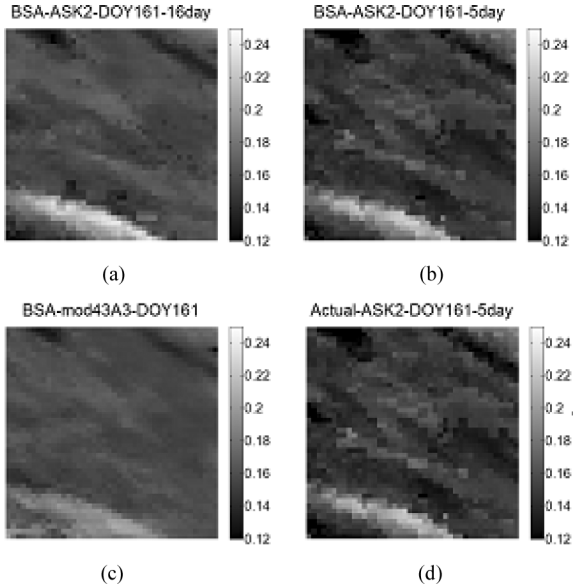

Fig. 4. ASK-2 retrieval (BSA and Actual Albedo) from (a), (b), (d) MOD09 versus (c) MOD43A3 for DOY161.

can explain the differences between 5-day and 16-day period retrieval for the latter two datasets. On the other hand, the result between 5-day and 16-day period retrieval for the first dataset seems much more consistent. The reason is no irrigation happened during this period and the corps in earlier growth stage grows not as fast as irrigation stage. It is also noted that MOD43A3 product has a smoother spatial distribution while there exist some speckles in ASK-2 inversion results. These may be explained by that MOD43A3 are sophisticated product with a complete set of constraints and singularity control, while the ASK-2 retrieval algorithm is only provisional. For the speckles occurs in Fig. 2(b) and (d), the retrieved albedos are higher than the surroundings. It is due to the MOD09 observation accumulated for these pixels are much less and not enough to attain a full inversion. While in AMBRALS, data from a prior known knowledge database is involved in the inversion as a compensation which helps the inversion reliable and stable even with limited observations, so its product MOD43A3 [Fig. 2(c)] looks much smoother. The results of WSA are very similar to those of BSA and will not be listed here.

For small-scale satellite-borne data validation, ASK-2 model is applied to CHRIS data containing 18 bands at about 18-m spatial resolution acquired on June 4th, 2008, at Yingke site. The five angular CHRIS acquisitions are assumed to take place within a 55° cone, as defined by a vector connecting the center of the Earth to the spacecraft. In this paper, four angular images $(0^\circ, \pm 36^\circ, 55^\circ)$ of 200×300 pixels are used to retrieve albedo in the area around Yingke site. Fig. 5 shows that the retrievals of actual shortwave albedo generally coincide with the false color composite image; bare soil gives higher albedo than cropland. Fig. 5(c) and (d) demonstrates the albedo retrieved from MOD09 data corresponding to the area of CHRIS image and acquired in five days around June 4th. It can be seen that the values' trend generally follows their counterparts from CHRIS; at the same time, differences exist due to the scale mismatch as well as the period difference.

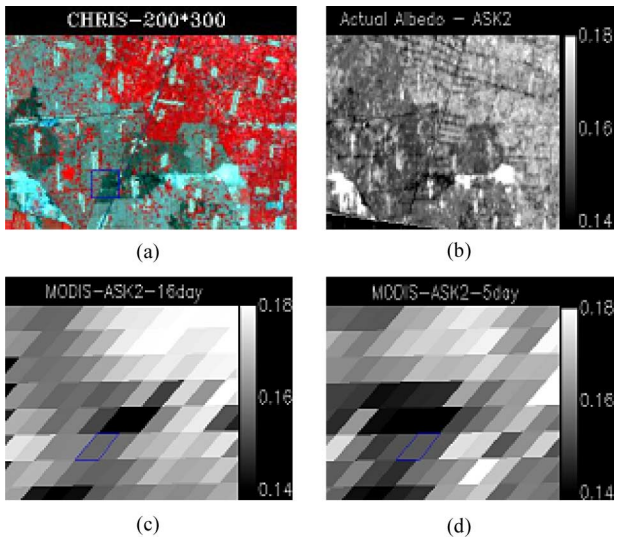

Fig. 5. ASK-2 (Actual Albedo) from (b) CHRIS versus (c), (d) MOD09.

TABLE X
ASK-2(A) AND ROSSLI(R) RETRIEVED ACTUAL SHORTWAVE ALBEDO FOR YINGKE SITE FROM CHRIS AND MOD09 VERSUS FIELD MEASUREMENTS

albedo	M	CHRIS point	CHRIS avg.	MOD09 -16days	MOD09 -5days	AWS	Obs.
WSA	A	0.1419	0.1492	0.1572	0.1349	-	-
	R	--	--	0.2011	0.196	-	-
BSA	A	0.1385	0.1554	0.1606	0.1505	-	-
	R	-	--	0.1701	0.1701	-	-
Actual	A	0.1397	0.1568	0.1601	0.1482	0.1204	0.1466
	R	--	--	0.196	0.1918		

albedometer measurements are not available for WSA & BSA
AMBRALS is only used for MODIS observation

Focused on the comparison of retrieved and observed albedo for Yingke site on June 4th, Table X demonstrates the shortwave albedo of different scale retrieval and *in situ* measurements for corn field. Note that the albedo from AWS record is lower; this is attributed to the irrigation on June 3rd on the eastern part the cropland, which greatly increases the soil moisture. Even though the portable albedometer location is very near to the AWS, the underlying corn is not irrigated when the measurement is taken and its value can indicate the albedo of nonirrigated part of the cropland. More specific illustration about the irrigation issue is given in Fig. 6, which gives the Albedo retrievals from CHRIS images centered in Yingke automatic weather station. The blue square region consists of 29×29 pixels corresponding to 1 MODIS pixel of 500-m resolution. On the eastern part of the square, some of the retrievals are found to be lower, so the image seems darker in these areas. These lower albedos indicate that the crop field of these pixels is irrigated.

With high resolution, the retrievals should be able to be compared with *in situ* measurement directly, while the retrievals with coarse resolution can not be compared with measurements directly. Instead, after downscale transform by aggregating pixels

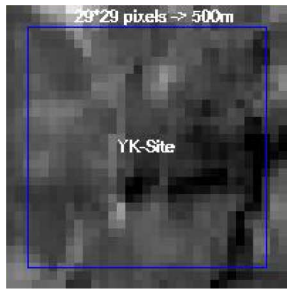

Fig. 6. Retrieval (actual albedo) from CHRIS.

circled out with the blue square in Fig. 6 to MODIS scale shown in Fig. 5(c) and (d), the average values can serve as bridge to connect MODIS retrievals with *in situ* measurements. Results show that the retrieved shortwave albedo from CHRIS agrees the AWS record best, whereas, due to scale mismatch, the retrievals from MODIS are much higher. Fortunately, the average value after aggregation of CHRIS pixels agrees the MODIS retrieval better. As a preliminary attempt to do scale transform, this paper just gives one example of single pixel validation for MODIS image. More investigation and validation need to be carried out in future.

V. SENSITIVITY ANALYSIS AND DISCUSSION

Generally speaking, retrieval accuracy is influenced by two factors: 1) deficiencies in the observed BRDF dataset, e.g., noise and poor sampling, and 2) capability of the model to represent the reality in the absence of noise. Sensitivity analysis is a common resort to address these problems. Usually, an "ideal" dataset is simulated with the model to represent the case of no noise in data and no model misfit; then, the "ideal" case is disturbed by noise or model misfit and the change of the inversion result is analyzed. Sensitivity analysis hints us how bad the model inversion result could go in practical situations. Robustness of model inversion, which means adequately small sensitivity to the disturbance, is a necessary feature when the inversion is to be applied to satellite remote-sensing data.

Here, a simulated BRDF dataset, referred as an "ideal" dataset, is created by applying the forward model, i.e., (9), with kernel coefficient in Table XI (inverted kernel coefficient from MODIS 16-day BRF of corn, wheat, desert, etc.) and observation angles as well as bands according to Section IV–A2. The results of model inversion include kernel coefficients, BSA, and WSA of each waveband or integrated to broadband. The ASK model is essentially more a semi-empirical model than a physical model, and the ultimate goal of this study is to propose an algorithm for albedo retrieval. Thus, the sensibility is analyzed only for albedo in this paper. Specifically, the actual albedo in Table XII is referred as the "true" value corresponding to the "ideal" dataset.

In order to judge the influence of disturbance to the retrieved albedo, the relative error is defined as

$$\varepsilon_r = \frac{|\alpha - \alpha_0|}{\alpha_0} \times 100\%$$

TABLE XI
ASK-2 AND ROSSLI RETRIEVED VIS ALBEDO FOR YINGKE SITE FROM CHRIS AND MOD09

albedo	ASK-2				RossLi	
	CHRIS point	CHRIS avg.	MOD09 -16days	MOD09-16days	MOD09 -16days	MO9 -5days
WSA	0.0591	0.0511	0.0388	0.0549	0.1039	0.2011
BSA	0.0634	0.0626	0.0657	0.0721	0.0888	0.1702
Actual	0.0644	0.0612	0.0614	0.0694	0.1014	0.1960

TABLE XII
ASK-2 AND ROSSLI RETRIEVED NIR ALBEDO FOR YINGKE SITE FROM CHRIS AND MOD09

albedo	ASK-2				RossLi	
	CHRIS point	CHRIS avg.	MOD09 -16days	MOD09-16days	MOD09 -16days	MO9 -5days
WSA	0.225	0.2645	0.2313	0.2597	0.3035	0.225
BSA	0.2137	0.2573	0.2354	0.2492	0.2564	0.2137
Actual	0.2152	0.2598	0.2351	0.2511	0.2959	0.2152

CHRIS point: retrieval for one pixel in CHRIS image
CHRIS avg.: average value after aggregating retrievals of 29*29 pixels centered in the point

TABLE XIII
RELATIVE ERROR OF ALBEDO WHEN RANDOM NOISES WERE ADDED

	α_0	Average ε_r of different noise level(%)			
		1% noise	2% noise	5% noise	10% noise
1	0.168141	1.077125	1.092827	1.509426	2.543625
2	0.168719	1.60335	1.653349	2.024432	3.087337
3	0.141081	2.155162	1.837586	2.995848	5.373382
4	0.220711	1.538224	1.55326	2.449064	4.526134
5	0.19007	2.129179	2.013893	2.443071	3.416594

TABLE XIV
RELATIVE ERROR OF ALBEDO GIVEN LIMITED NUMBER OF ANGULAR SAMPLES

	Average ε_r of different number of angular samples (%)					
	1 angle	2 angles	3 angles	4 angles	5 angles	10 angles
1	4.98408	2.54852	3.09452	1.86810	1.17535	1.33813
2	8.27777	3.21581	2.27991	2.87749	2.04820	1.22659
3	6.77508	3.80407	3.01929	2.78027	2.56295	1.60796
4	8.86267	4.20750	2.35852	1.85099	2.16816	2.24145
5	11.1071	5.97065	4.79599	2.99262	3.29378	2.47592

where α_0 is the "true" albedo corresponding to the "ideal" dataset, and α is the inversion result after adding some kind of disturbance.

A. Sensitivity to Random Noise in the BRF Dataset

Noises found in remote-sensing data can be random or systematic, which may come from erroneous calibration or atmosphere correction. Like others algorithms for land surface albedo retrieval, the input should be adequately calibrated, georectified, and atmospheric corrected directional reflectance. Thus, only the random noises are considered in this paper.

Table XIII lists the relative error of albedo when different levels of random noises were added into the "ideal" BRF dataset. The random noises are first generated according to Gaussian distribution of zero mean and unit deviation, then, multiplied by the noise level and the value of BRF. For each target and each noise level, 100 times of noise simulation are run to derive the average relative error. Results show that all of the figures for average relative error from different noise level are smaller than 5.5%. Then, it can be concluded that this algorithm is not sensitive to random noises in the observed BRFs. This merit makes it possible to use ASK to get stable and reliable results even with contaminated observations.

B. Model Performance When Using Poorly Sampled Data

For current MODIS albedo product of NASA, a 16-day observation period is needed to construct the BRF dataset, corresponding to a complete cycle of orbits for the platform. While a shorter period is desirable, cloud cover statistics show that shorter periods (e.g., 8 days) will significantly reduce the number of pixels with sufficient observations for accurate BRDF inversion. The ASK model with both spectral and directional kernels will potentially be able to exploit data with limited directional sampling to derive albedo.

In Sections IV–A2 and IV–B2, the capability of using the ASK-2 model to generate an albedo map from five days of MODIS-Terra and MODIS-Aqua data (10 observations) have been demonstrated. This enables the possibility of increasing temporal resolution of albedo product. In practice, we must face the situation of even less observations because of cloud. So, the performance of ASK model given limited number of angular samples is tested.

Table XIV lists the relative error of albedo with different numbers of angular samples. The angular samples are randomly selected out from the "ideal" dataset added 1% noise. Thus, they are a subset of possible MODIS view angles. As in Section V–A, 100 tests are run for each target and sample number to derive statistics.

Since ε_r is derived from 100 times' random sampling, typical angular distributions can be assumed to be represented. Here, to simplify the analysis, we focus on the model's performance under different angular number without considering the angular distribution. From the result listed in Table XIV, all of the figures are smaller than 5% when the number of angle is more than three from which conclusion can be drawn that the algorithm is feasible for even as few as three well-distributed angular observations. This is owing to the joint inversion of multispectra and multi-angular data which release the need of angular observations in the traditional way of constructing function against each waveband separately.

C. Sensitivity to Inaccurate Component Spectra

An important aspect of error source in albedo retrieval is the inability of model to fit noise-free data or to extrapolate to sun/view angles beyond the range of observation. Like other models, ASK model is compromise between accuracy and model simplicity. However, ASK model can be viewed as an extension of the kernel-driven BRDF model adopted by AMBRALS [53],

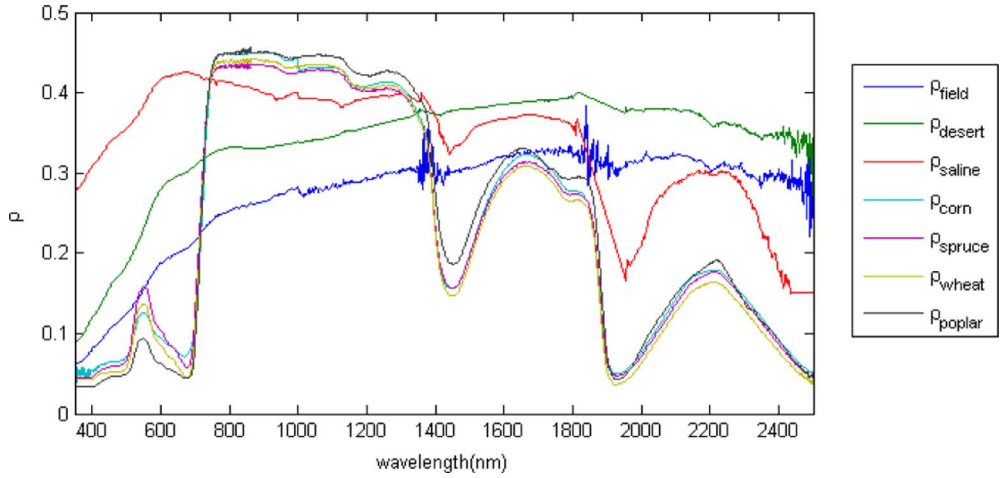

Fig. 7. Reflectance of YK field soil, semi-desert, salinized soil, corn, Norway spruce, wheat, and poplar.

TABLE XV
RELATIVE ERROR OF ALBEDO WHEN USING DIFFERENT COMPONENT SPECTRA

	Average ε_r of using different component spectra (%)				
	Semi-desert	Salinized soil	Norway spruce	Wheat	Poplar
1	0.760125	0.595168	0.524637	0.509553	1.990638
2	0.4015	0.698974	0.654655	2.973082	2.493174
3	2.130682	1.678664	2.69548	1.459746	1.433466
4	6.687917	7.518507	0.579843	0.476658	0.833559
5	1.270213	1.693254	0.44819	1.366409	1.234392

which has been proven to be globally applicable in literature. Thus, in this paper, we believe that ASK model is also a reliable model and direct our attention to more important analysis. As mentioned above, ASK model introduces component spectra from *a priori* database. Then, the most probable source of uncertainty in global albedo retrieval may come from the fact that component spectra can not be accurately provided all the time. Below, the impact of inaccurate component spectra to retrieved albedo is analyzed.

Unlike satellite observations, inaccuracy in component spectra should not be treated as random noise. Here spectra of other types of soil or plant species are used in the process of model inversion instead of that used in forward simulation. In Section IV–A, the component spectral data are *in situ* measurements of soil and corn leaf in Yingke experiment station. Now, another two typical soil spectra from Heihe experiment are chosen, one is collected in the semi-desert area near Huazhaizi, the other is collected for the salinized soil near Linze Grassland experiment station. For leaf spectra, reflectance and transmittance of corn, Norway spruce, wheat and poplar in the dataset of Lopex93 are chosen [69]. Fig. 7 shows the component spectra of different types.

Table XV lists the relative error of albedo when using inaccurate component spectra. For the sake of simplicity, only one component spectrum is changed in each test, i.e., either the soil reflectance or the leaf reflectance and transmittance are replaced.

It can be seen from Table XV that, in all cases, the relative errors of albedo do not exceed 3% when the leaf spectra of corn are replaced by other species. This may be explained by the similarity of leaf spectra for different species. As for inaccurate soil spectra, they cause larger error in albedo especially in the case of desert while there is little vegetation coverage. However, compared with the obvious differences between the component spectra used in forward model simulation and that used in inversion, the errors in retrieved albedo are smaller and, in most cases, acceptable. This indicates that the ASK model can adjust the inverted kernel coefficients to compensate for inaccurate component spectra from which their influence on albedo retrieval is minimized. It is actually an advantage of using empirical or semi-empirical model.

Anyway, it is strongly recommended to use the appropriate component spectral for BRDF and albedo inversion in regional or global applications. It proposes the necessity of constructing *a priori* database for spectra of typical soils and typical leaves, as well as classification map indicating which spectrum should be chosen for certain pixel.

D. Applicability of ASK Model at Global Scale

For a preliminary test of ASK model's applicability at global scale, the POLDER-3/PARASOL BRDF dataset are employed. It provides BRF with 6-km resolution derived from POLDER-3 observation for different kinds of cover types around the earth from November 2005 to October 2006. BRF data of 22 kinds of surface cover are chosen based on the coordination of the Global Land Cover 2000 (GLC2000) project accumulated during July 2006. For each surface cover, observations for different locations around the earth are included. Table XVI shows the maximum, average, and minimum fitting RMSE of data accumulated at different locations for each cover type. Note that, for all of the surface types except ice, the average value are under 4%, from which we can conclude that the fitting ability of ASK mode is applicable for most of the surface types. As for the worst performance, the maximum RMSE value can reach more than 20%, which obviously cannot be accepted. So, cautious consideration must be given to surface types such as ice or water, different model should be employed.

TABLE XVI
AVERAGE, MINIMUM, AND MAXIMUM FITTING RMSES FOR POLDER-3/PARASOL BRDF

	ASK-2 fitting RMSE		
Surface_type	Avg.	Min	Max
1 Tree Cover, broadleaved, evergreen;	0.02474	0.01450	0.05031
2 Tree Cover, broadleaved, deciduous, closed;	0.01653	0.00731	0.02984
3 Tree Cover, broadleaved, deciduous, open;	0.02356	0.01433	0.03935
4 Tree Cover, needle-leaved, evergreen;	0.01407	0.00755	0.02689
5 Tree Cover, needle-leaved, deciduous;	0.01720	0.00879	0.03081
6 Tree Cover, mixed leaf type;	0.01605	0.01010	0.02941
7 Tree Cover, regularly flooded, fresh;	0.02460	0.01073	0.04209
8 Tree Cover, regularly flooded, saline,	0.02679	0.01218	0.04961
9 Mosaic: Tree cover / Other natural vegetation;	0.01842	0.00641	0.03972
10 Tree Cover, burnt;	0.01689	0.01050	0.02684
11 Shrub Cover, closed-open, evergreen	0.02128	0.01135	0.05631
12 Shrub Cover, closed-open, deciduous	0.02335	0.00692	0.04624
13 Herbaceous Cover, closed-open;	0.02367	0.00793	0.03907
14 Sparse Herbaceous or sparse shrub cover;	0.02815	0.01172	0.04858
15 Regularly flooded shrub and/ or herbaceous cover;	0.02495	0.01060	0.07790
16 Cultivated and managed areas;	0.02166	0.00873	0.05455
17 Mosaic: Cropland / Tree Cover / Other Natural Vegetation;	0.02398	0.00727	0.04068
18 Mosaic: Cropland / Shrub and/ or Herbaceous cover;	0.01726	0.00563	0.03984
19 Bare Areas;	0.03728	0.00694	0.08843
20 Water Bodies (natural & artificial);	0.02139	0.00622	0.12069
21 Snow and Ice (natural & artificial);	0.18766	0.01030	0.41106
22 Artificial surfaces and associated areas	0.01667	0.00635	0.05589

It can be concluded from this analysis that, for developing an algorithm applicable on a global scale, not only the database for component spectra should be constructed, but also the various cover types should be considered. Moreover, it means that more kernel functions need to be derived, and their appropriate combination for each land cover type should be discovered.

VI. CONCLUSION AND DISCUSSION

This paper proposes a new angular and spectral kernel-based BRDF model (ASK model), which have three advantages. First, the new model is operational in both angular and spectral dimension with component spectra added into kernel functions. This makes it possible for joint inversion of multiband and multi-angular remote sensing data. As kernel coefficients are independent from wavelength, to use more spectral bands means increasing the number of equations without bringing new unknown variables. Therefore, it enables us to conduct robust albedo retrieval with less angular sampling, i.e., short period for product renewal. Second, this new model may be used to integrate kernels in both angular and spectral dimension to calculate broadband albedo. Third, taking advantage of the wavelength independence of kernel coefficients, multisource remote sensed data of different satellite can be jointly used in the inversion despite of the spectral band differences.

As an extension of the kernel-driven BRDF model, ASK model is a semi-empirical model also. Instead of pursuing the accuracy of inverted kernel coefficients, the value of this model should be examined in its ability to fit BRDF observations, to interpolate and extrapolate in angular or spectral domain, and to derive albedo. The validations in Sections IV–A and IV–B show that the ASK model is applicable. Additionally, ASK model requires five free variables, two more than AMBRALS, which means that more mathematical functions are needed to get a good fit and makes ASK seem to be more complex. As a matter of fact, this deficiency can be compensated by the joint-inversion coupling spectral and angular information from multisource remote sensing data.

Although we present the ASK model as potentially better way to retrieve albedo than the original kernel-driven BRDF model in the AMBRALS algorithm, we do not expect it can replace AMBRALS immediately. Much more research should be done before actually applying it to global product generation, for example, building the database for component spectra of typical land cover is a big task. As it is a promising direction to combine multisource remote-sensing data to retrieve land–surface parameters with much more high accuracy, we will continue our research based on the presented work in this paper.

ACKNOWLEDGMENT

The authors would like to thank the many scientists and students who carried out the field measurement in WATER to support the validation of this work, we also extend our thanks to LSCE and POSTEL who elaborated and provide the POLDER-3/PARASOL BRDFs databases; Dragon Project and Pro. Fan Wenjie who provided and processed CHRIS image; and NASA who provides various MODIS products.

REFERENCES

[1] "Implementation Plan for the Global Observing System for Climate in Support of the UNFCCC," Rep. GCOS–92 (WMO/TD No. 1219), 2004, pp. 136p–.
[2] J. C. Stroeve, J. E. Box, C. Fowler, T. Haran, and J. Key, "Intercomparison between in situ and AVHRR polar pathfinder-derived surface albedo over Greenland," *Remote Sens Environ*, vol. 62, pp. 262–276, 2001.
[3] B. Pinty, T. Lavergne, T. Kaminski, O. Aussedat, R. Giering, N. Gobron, M. Taberner, M. M. Verstraete, M. Vo Beck, and J. L. Widlowski, "Partitioning the solar radiant fluxes in forest canopies in the presence of snow," *J. Geophys. Res.*, vol. 113, 2008.
[4] "Summary Report of the Eight Session of the GCOS/GTOS/Terrestrial Observation Panel for Climate," Rep. GCOS-93/GTOS-35, (WMO/TD No. 1238), 2004, pp. 23–.
[5] A. Weiss, T. J. Arkebauer, and E. A. W. Shea, "Evaluation of an algorithm for predicting albedo in heliotropic crops," *Agr. Syst.*, vol. 67, pp. 856–860, 2001.
[6] F. E. Nicodemus, J. C. Richmond, J. J. Hsia, I. W. Ginsberg, and T. Limperis, "Geometrical considerations and nomenclature for reflectance," Nat. Bureau of Standards, 1977.
[7] J. V. Martonchik, C. J. Bruegge, and A. H. Strahler, "A review of reflectance nomenclature used in remote sensing," *Remote Sens. Rev.*, vol. 19, pp. 9–20, 2000.
[8] G. S. Strub, M. E. Schaepman, T. H. Painter, S. Dangel, and J. V. Martonchik, "Reflectance quantities in optical remote sensing-definitions and case studies," *Remote Sens. Environ.*, vol. 109, pp. 107–117, 2006.

[9] M. J. Barnsley, P. Lewis, M. Sutherland, and J. P. Muller, "Estimating land surface albedo in the HAPEX-Sahel southern super-site: inversion of two BRDF models against multiple angle ASAS images," *J. Hydrol.*, vol. 113, pp. 24–39, 1997.

[10] R. A. De Abreu, J. Key, J. A. Maslanik, M. C. Serreze, and E. F. LeDrew, "Comparison of in situ and AVHRR-derived broadband albedo over Arctic sea ice," *Arctic*, vol. 47, pp. 288–297, 1994.

[11] A. H. Strahler, "Vegetation canopy reflectance modelling- recent developments and remote sensing perspectives," *Remote Sens. Rev.*, vol. 15, pp. 179–194, 1997.

[12] J. R. Key and A. J. Schweiger, "Tools for atmospheric radiative transfer: Streamer and FluxNet.," *Comput. Geosci.-U.K.*, vol. 46, pp. 413–423, 1998.

[13] J. T. Suttles, R. N. Green, P. Minnis, G. L. Smith, W. F. Staylor, B. A. Wielicki, I. J. Walker, D. F. Young, V. R. Taylor, and L. L. Stowe, Angular radiation models for Earth-atmosphere system. volume 1: Shortwave radiation," 1988.

[14] O. Pokrovsky and J. Roujean, "Land surface albedo retrieval via kernel-based BRDF modeling: I. Statistical inversion method and model comparison," *Remote Sens. Environ.*, vol. 84, pp. 120–142, 2003.

[15] A. H. Strahler, J. P. Muller, W. Lucht, C. B. Schaaf, T. Tsang, F. Gao, X. Li, P. Lewis, and M. J. Barnsley, "MODIS BRDF/albedo product: algorithm theoretical basis document version 5.0," *MODIS Documentation*, 1999.

[16] C. L. Walthall, J. M. Norman, J. M. Welles, G. Campbell, and B. L. Blad, "Simple equation to approximate the bidirectional reflectance from vegetative canopies and bare soil surfaces," *Appl. Opt.*, vol. 24, pp. 383–387, 1985.

[17] F. Cabot and G. Dedieu, "Surface albedo from space: Coupling bidirectional models and remotely sensed measurements," *J. Geophys. Res.*, vol. 102, pp. 19645–19664, 1997.

[18] M. J. Barnsley, P. D. Hobson, A. H. Hyman, W. Lucht, J. Muller, and A. H. Strahler, "Characterizing the spatial variability of broadband albedo in a semidesert environment for MODIS validation," *Remote Sens. Environ.*, vol. 74, pp. 85–98, 2000.

[19] C. B. Schaaf, J. Martonchik, B. Pinty, Y. Govaerts, F. Gao, A. Lattanzio, J. Liu, A. Strahler, and M. Taberner, "Retrieval of surface albedo from satellite sensors," *Adv. Land Remote Sens.: Syst., Modeling, Inversion and Application*, pp. 219–243, 2008.

[20] B. Pinty, F. Roveda, M. M. Verstraete, N. Gobron, Y. Govaerts, J. V. Martonchik, D. J. Diner, and R. A. Kahn, "Surface albedo retrieval from Meteosat—1. Theory," *J. Geophys. Res.*, vol. 105, 2000.

[21] B. Pinty, F. Roveda, M. M. Verstraete, N. Gobron, Y. Govaerts, J. V. Martonchik, D. J. Diner, and R. A. Kahn, "Surface albedo retrieval from Meteosat-2. Applications," *J. Geophys. Res.*, vol. 105, 2000.

[22] Y. M. Govaerts, A. Lattanzio, B. Pinty, and J. Schmetz, "Consistent surface albedo retrieval from two adjacent geostationary satellites," *Geophys. Res. Lett.*, vol. 31, 2004, L15201.

[23] Y. M. Govaerts, B. Pinty, M. Taberner, and A. Lattanzio, "Spectral conversion of surface albedo derived from Meteosat first generation observations," *IEEE Geosci. Remote Sens. Lett.*, vol. 3, no. 1, pp. 23–27, Jan. 2006.

[24] W. van Leeuwen and J. L. Roujean, "Land surface albedo from the synergistic use of polar (EPS) and geo-stationary (MSG) observing systems—An assessment of physical uncertainties," *Remote Sens. Environ.*, vol. 81, pp. 273–289, 2002.

[25] B. Geiger, D. Lajas, L. Franchistéguy, D. Carrer, J. L. Roujean, S. Lanjeri, and C. Meurey, "The Land-SAF Surface Albedo and Downwelling Shortwave Radiation Flux Products," 2005.

[26] J. V. Martonchik, D. J. Diner, R. A. Kahn, T. P. Ackerman, M. M. Verstraete, B. Pinty, and H. R. Gordon, "Techniques for the retrieval of aerosol properties over land and ocean using multiangle imaging," *IEEE Trans. Geosci. Remote Sens.*, vol. 36, no. 4, pp. 1212–1227, Jul. 1998.

[27] J. V. Martonchik, D. J. Diner, B. Pinty, M. M. Verstraete, R. B. Myneni, Y. Knyazikhin, and H. R. Gordon, "Determination of land and ocean reflective, radiative, and biophysical properties using multiangle imaging," *IEEE Trans. Geosci. Remote Sens.*, vol. 36, no. 4, pp. 1266–1281, Jul. 1998.

[28] J. V. Martonchik, B. Pinty, and M. M. Verstraete, "Note on 'An Improved Model of Surface BRDF-Atmospheric Coupled Radiation'," *IEEE Trans. Geosci. Remote Sens.*, vol. 40, no. 7, pp. 1637–1639, Jul. 2002.

[29] D. Rutan, T. Charlock, F. Rose, S. Kato, S. Zentz, and L. Coleman, "Global surface albedo from CERES/TERRA surface and atmospheric radiation budget (SARB) data product," in *Proc. 12 Conf. Atmosph. Radiation (AMS)*, 2006, pp. 10–14.

[30] M. Leroy, J. L. Deuzé, F. M. Bréon, O. Hautecoeur, M. Herman, J. C. Buriez, D. Tanré, S. Bouffies, P. Chazette, and J. L. Roujean, "Retrieval of atmospheric properties and surface bidirectional reflectances over land from POLDER/ADEOS," *J. Geophys. Res.*, vol. 102, pp. 17–37, 1997.

[31] C. Bacour and F. BrIon, "Variability of biome reflectance directional signatures as seen by POLDER," *Remote Sens. Environ.*, vol. 21, pp. 284–285, 2005.

[32] P. Bicheron and M. Leroy, "Bidirectional reflectance distribution function signatures of major biomes observed from space," *J. Geophys. Res.*, vol. 105, pp. 626–669, 1998, 26, 681.

[33] F. Maignan, F. M. Bréon, and R. Lacaze, "Bidirectional reflectance of Earth targets: Evaluation of analytical models using a large set of spaceborne measurements with emphasis on the Hot Spot," *Remote Sens. Environ.*, vol. 90, pp. 210–220, 2004.

[34] O. Hautecoeur and M. M. Leroy, "Surface bidirectional reflectance distribution function observed at global scale by POLDER/ADEOS," *Geophys. Res. Lett.*, vol. 25, pp. 4197–4200, 1998.

[35] J. P. Muller, "BRDF/albedo retrieval," 2008.

[36] W. Lucht, A. H. Hyman, A. H. Strahler, M. J. Barnsley, P. Hobson, and J. P. Muller, "A comparison of satellite-derived spectral albedos to ground-based broadband albedo measurements modeled to satellite spatial scale for a semidesert landscape," *Remote Sens. Environ.*, vol. 74, pp. 85–981, 2000.

[37] F. Gao, C. B. Schaaf, A. H. Strahler, A. Roesch, W. Lucht, and R. Dickinson, "MODIS bidirectional reflectance distribution function and albedo climate modeling grid products and the variability of albedo for major global vegetation types," *J. Geophys. Res*, vol. 110, 2005, Art. ID D01104.

[38] C. B. Schaaf, F. Gao, A. H. Strahler, W. Lucht, X. Li, T. Tsang, N. C. Strugnell, X. Zhang, Y. Jin, J. Muller, P. Lewis, M. Barnsley, P. Hobson, M. Disney, G. Roberts, M. Dunderdale, C. Doll, R. P. D'Entremontf, B. Hu, S. Liangh, J. L. Privettei, and D. Royh, "First operational BRDF, albedo nadir reflectance products from MODIS," *Remote Sens. Environ.*, vol. 105, pp. 155–171, 2002.

[39] B. Pinty, M. Taberner, S. Liang, Y. Govaerts, J. V. Martonchik, A. Lattanzio, C. B. Schaaf, M. M. Verstraete, R. E. Dickinson, and N. Gobron, "Intercomparison of surface albedo products from various spaceborne sensors," in *Proc. Workshop Inter-Comparison large Scale Opt. Infrared Sensors*, Noordwijk, The Netherlands, Oct. 12–14, 2004.

[40] F. Baret, C. Schaaf, J. Morisette, and J. Privette, "Report on the Second International Workshop on Albedo Product Validation," *The Earth Observer*, vol. 17, pp. 13–17, 2005.

[41] S. Liang, H. Fang, M. Chen, C. J. Shuey, C. Walthall, C. Daughtry, J. Morisette, C.Validating MODIS land surface reflectance and albedo products: methods and preliminary results Schaaf, and A. Strahler, "Validating MODIS land surface reflectance and albedo products: methods and preliminary results," *Remote Sens Environ*, vol. 83, pp. 3–15, 2002.

[42] Y. Jin, C. B. Schaaf, F. Gao, X. Li, A. H. Strahler, W. Lucht, and S. Liang, "Consistency of MODIS surface bidirectional reflectance distribution function and albedo retrievals: 1. Algorithm performance," *J. Geophys. Res.*, vol. 108, pp. 4158–, 2003.

[43] Y. Shuai, C. B. Schaaf, A. H. Strahler, J. Liu, and Z. Jiao, "Quality assessment of BRDF/albedo retrievals in MODIS operational system," *Geophys. Res. Lett.*, vol. 35, pp. 1–5407, 2008.

[44] W. Greuell and J. Oerlemans, "Narrowband-to-broadband albedo conversion for glacier ice and snow: equations based on modeling and ranges of validity of the equations," *Remote Sens. Environ.*, vol. 82, pp. 48–63, 2004.

[45] S. Liang, "Narrowband to broadband conversions of land surface albedo I: Algorithms," *Remote Sens. Environ.*, vol. 113, pp. 24–39, 2001.

[46] S. Liang, C. J. Shuey, A. L. Russ, H. Fang, M. Chen, C. L. Walthall, C. S. T. Daughtry, and R. Hunt, "Narrowband to broadband conversions of land surface albedo: II. Validation," *Remote Sens. Environ.*, vol. 76, pp. 213–238, 2003.

[47] H. Fang, S. Liang, H. Y. Kim, T. J. R, C. L. Schaaf, A. H. Strahler, and R. E. Dickinson, "Developing a spatially continuous 1 km surface albedo data set over North America from Terra MODIS products," *Geophys. Res.*, vol. 112, pp. 10–1029, 2007.

[48] Y. M. Govaerts, A. Lattanzio, M. Taberner, and B. Pinty, *Remote Sens. Environ.*, vol. 64, no. 08, pp. 139–145.

[49] P. Lewis and M. J. Barnsley, "Influence of the sky radiance distribution on various formulations of the Earth surface albedo," presented at the Int. Symp. Physical Meas. and Signatures in Remote Sens, Val d'Isere, France, 1994.

[50] E. Vermote, D. Tanre, J. L. Deuze, M. Herman, and J. J. Morcrette, "Second simulation of the satellite signal in the solar spectrum (6S)," *6S User Guide Version*, vol. 2, 1997.
[51] W. Lucht, C. B. Schaaf, and A. H. Strahler, "An algorithm for the retrieval of albedo from space using semiempirical BRDF models," *IEEE Trans. Geosci. Remote Sens.*, vol. 38, no. 2, pp. 977–998, Mar. 2000.
[52] X. W. Li, F. Gao, and Q. Liu, "Validation of a new GO kernel and inversion of land surface albedo by kernel-driven model (2)," *Remote Sensing (in Chinese)*, vol. 4, pp. 8–15, 2000.
[53] W. Wanner, X. Li, and A. H. Strahler, *J. Geophys. Res.*, vol. 100, 1995.
[54] X. Li and A. H. Strahler, "Geometric-optical bidirectional reflectance modeling of the discrete crown vegetation canopy: Effect of crown shape and mutual shadowing," *IEEE Trans. Geosci. Remote Sens.*, vol. 30, no. 2, pp. 276–292, Mar. 1992.
[55] R. P. D'Entremont, C. B. L. W. Schaaf, and A. H. Sfrahler, "Retreval of red spectral albedo and bidirectional reflectance from 1-km^2 satellite observations for the New England region," *J. Geophys. Res.*, vol. 104, pp. 6329–6339, 1999.
[56] F. Gao, C. B. Schaaf, A. H. Strahler, Y. Jin, and X. Li, "Detecting vegetation structure using a kernel-based BRDF model," *Remote Sens. Environ.*, vol. 111, pp. 36–50, 2003.
[57] W. Huang, Z. Niu, J. Wang, L. Liu, C. Zhao, and Q. Liu, "Identifying crop leaf angle distribution based on two-temporal and bidirectional canopy reflectance," *IEEE Trans. Geosci. Remote Sens.*, vol. 44, no. 12, pp. 3601–, Dec. 2006.
[58] S. Liu, Q. Liu, Q. Liu, and X. Li, "Multi-angles & multi-spectrum kernel-driven model and its application in the research of BRDF," *J. Beijing Normal Univ. (Natur. Sci.) (China)*, vol. 43, pp. 309–313, 2007.
[59] I. U. Ross, *The Radiation Regime and Architecture of Plant Stands*. Berlin, Germany: Springer-Verlag, 1981.
[60] J. L. Roujean, "A bidirectional reflectance model of the Earth's surface for the correction of remote sensing data," *J. Geophys. Res.*, vol. 97, pp. 20–455, 1992.
[61] W. C. Snyder and Z. Wan, "BRDF models to predict spectral reflectance and emissivity in the thermal infrared," *IEEE Trans. Geosci. Remote Sens.*, vol. 36, no. 1, pp. 214–225, Jan. 1998.
[62] B. Hapke, "Bidirectional reflection spectroscopy 1. Theory," *J. Geophys. Res.*, vol. 86, pp. 3039–3054, 1981.
[63] E. Muller and H. DIcamps, "Modeling soil moisture-reflectance," *Remote Sens Environ.*, vol. 131, pp. 227–238, 2001.
[64] P. Lewis, "The utility of linear kernel-driven BRDF models in global BRDF and albedo studies," in *Proc. Int. Geosci. Remote Sens. Symp.*, 1995, vol. 95, pp. 1186–1187.
[65] S. Liang, A. H. Strahler, and C. Walthall, "Retrieval of land surface albedo from satellite observations: A simulation study," *J. Appl. Meteorol.*, vol. 38, pp. 712–725, 1999.
[66] J. Stroeve, A. Nolin, and K. Steffen, "Comparison of AVHRR-derived and in situ surface albedo over the greenland ice sheet," *Remote Sens. Environ.*, vol. 9, pp. 143–164, 1997.
[67] B. Hu, W. Lucht, X. Li, and A. H. Strahler, "Validation of kernel-driven semiempirical models for the surface bidirectional reflectance distribution function of land surfaces," *Remote Sens. Environ.*, vol. 113, pp. 24–39, 1997.
[68] R. Deng, G. Tian, Q. Liu, and X. Xin, "Research on remote sensing model for soil water on rough surface," *J. Remote Sens. (China)*, vol. 18, pp. 75–80, 2004.
[69] B. Hosgood, S. Jacquemoud, G. Andreoli, J. Verdebout, G. Pedrini, and G. Schmuck, "Leaf optical properties experiment 93 (LOPEX93)," Ispra, Italy, 1995.

Qinhuo Liu received the B.Sc. degree in hydrogeology and engineering geology from Southwest Jiaotong University, Chengdu, Sichuan, China, in 1988, and the M.Sc. degree in cartography and remote sensing and the Ph.D. degree in atmospheric physics from Peking University, Beijing, China, in 1994 and 1997, respectively.

He visited INRA of France in 1998, Boston University, Boston, MA, in 1999, and the University of Maryland, College Park, in 2003 as a Visiting Scholar. Since 1997, he has been with the Institute of Remote Sensing Applications, Chinese Academy of Sciences, Beijing, where he is currently a Professor and the Deputy Director of the State Key Laboratory of Remote Sensing Science. His research interests include radiation-transfer model of land surface and quantitative remote-sensing inversion, assimilation, and applications.

Sihan Liu received the B.A. degree from Beijing Normal University, Beijing, China, in 2005. She is currently working toward the Ph.D. degree at the Institute of Remote Sensing Applications, Chinese Academy of Sciences, Beijing.

Her main research activities are in radiative transfer simulation, modeling of bidirectional reflectance distribution function and surface albedo retrieval.

Qiang Liu received the B.S. degree in computational mathematics from Beijing University, Beijing, China, in 1997 and the Ph.D. degree in cartography and remote sensing from the Institute of Remote Sensing Applications, Chinese Academy of Sciences, Beijing, in 2002.

He is currently an Associate Scientist with the Institute of Remote Sensing Applications, Chinese Academy of Sciences. His main research interest is multi-angular remote-sensing modeling and inversion, with applications in agriculture, ecosystems, and forest and urban studies.